Developing a combat-relevant translatable large animal model of heterotopic ossification

Richard T. Epperson [a,b,*], Brad M. Isaacson [b,c,d], David L. Rothberg [a,b], Raymond E. Olsen [b], Brooke Kawaguchi [a,b], John M. Maxwell [a,b], Mary Dickerson [e], Paul F. Pasquina [d,f], John Shero [d,g], Dustin L. Williams [a,b,d,h,i]

[a] University of Utah, Bone & Biofilm Research Laboratory, Salt Lake City, UT, United States of America
[b] University of Utah, Department of Orthopaedics, Salt Lake City, UT, United States of America
[c] The Geneva Foundation, Tacoma, WA, United States of America
[d] The Center for Rehabilitation Sciences Research, Uniformed Services University, Bethesda, MD, United States of America
[e] University of Utah, Office of Comparative Medicine, Salt Lake City, UT, United States of America
[f] Department of Rehabilitation, Walter Reed National Military Medical Center, Bethesda, MD, United States of America
[g] Extremity Trauma Center of Excellence, Joint Base San Antonio Fort Sam Houston, San Antonio, TX, United States of America
[h] University of Utah, Department of Pathology, Salt Lake City, UT, United States of America
[i] University of Utah, Department of Bioengineering, Salt Lake City, UT, United States of America

ARTICLE INFO

ABSTRACT

Heterotopic ossification (HO) refers to ectopic bone formation, typically in residual limbs following trauma and injury. A review of injuries from Operation Iraqi Freedom (OIF) and Operation Enduring Freedom (OEF) indicated that approximately 70% of war wounds involved the musculoskeletal system, largely in part from the use of improvised explosive devices (IED) and rocket-propelled grenades (RPG). HO is reported to occur in approximately 63%–65% of wounded warriors from OIF and OEF. Symptomatic HO may delay rehabilitation regimens since it often requires modifications to prosthetic limb componentry and socket size. There is limited evidence indicating a mechanism for preventing HO. This may be due to inadequate models, which do not produce HO bone structure that is morphologically similar to HO samples obtained from wounded warfighters injured in theatre. We hypothesized that using a high-power blast of air (shockwave) and simulated battlefield trauma (i.e. bone damage, tourniquet, bacteria, negative pressure wound therapy) in a large animal model, HO would form and have similar morphology to ectopic bone observed in clinical samples. Initial radiographic and micro-computed tomography (CT) data demonstrated ectopic bone growth in sheep 24 weeks post-procedure. Advanced histological and backscatter electron (BSE) analyses showed that 5 out of 8 (63%) sheep produced HO with similar morphology to clinical samples. We conclude that not all ectopic bone observed by radiograph or micro-CT in animal models is HO. Advanced histological and BSE analyses may improve confirmation of HO presence and morphology, which we demonstrated can be produced in a large animal model.

1. Introduction

Heterotopic ossification (HO) is a pathology described as ectopic bone that develops outside natural skeleton borders, typically in residual limbs and/or peri-articular regions (Isaacson et al., 2010; Brown et al., 2010). The direct cause of HO is not fully understood, however, is categorized in three separate forms; (1) Traumatic HO, which can be induced by bone fracture, burns and following surgical procedures (including total joint replacement). (2) Neurogenic HO which appears following spinal and/or head injuries. (3) Genetic/Hereditary HO for example, fibrodysplasia ossificans progressiva and progressive osseous hetero plasia are both shown to trigger HO growth (Balboni et al., 2006; Shore and Kaplan, 2010; van Leeuwen et al., 2016). In addition to the factors listed above, Traumatic HO is also induced by soft tissue damage and inflammation (Errico et al., 1984; Bayley, 1979), and is frequently observed after combat-related trauma to service members with blast injuries (Potter and Scoville, 2006). HO growth can be extra-skeletal as well as stemming from the periosteum or resected limbs as observed in

amputees (Henrot et al., 2000; Atkinson et al., 2010). Radiographic and histological evaluation of HO is predominantly reported as being mature cancellous bone within a cortical shell (Shehab et al., 2002). However, other studies have demonstrated that, although the HO has similarities to cancellous bone, the structure is less defined than normal bone and has slight, but important differences. These studies show that mature HO bone has irregular distribution of fibrils in a non-osteon like pattern with occasional haversian systems (osteons) as well as irregular distributed osteocytes that help distinguish HO from normal bone (Rossier et al., 1973; Ohlmeier et al., 2019). Surgically excised samples from wounded warriors furthered this analysis and elucidated HO morphology by backscatter electron (BSE) imaging, and confirmed that the HO composition is a unique bone structure. The traumatic HO bone that manifested in wounded warriors was shown to be a complex hybrid trabecular-like structure with osteon remodeling, as well as hyper-mineralized regions of woven bone (Isaacson et al., 2011a; Isaacson et al., 2016).

It is reported that HO growth affects 63%–65% of wounded warriors who suffer limb loss or major extremity trauma (Forsberg et al., 2009; Forsberg and Potter, 2010; Potter et al., 2007). The development of HO delays rehabilitation regimens, particularly due to the pain associated with exercise or movement. Ectopic bone that develops in soft tissues causes tenderness and even debilitates movement, requiring modifications to prosthetic limb componentry and socket size, or prevents their use altogether (Potter et al., 2010; Dudek et al., 2003).

Small animal models provide a benchmark of information, suggesting that trauma, amputation and bacterial contamination all influence ectopic bone growth. Rats and rabbits are commonly used for HO research, yet their bone growth rates are 600% and 40% higher than humans, respectively (Marcus et al., 2013; Isaacson et al., 2011b). Increased remodeling rates limit the translatability of these models, in particular as HO is documented to be more metabolically active than non-pathological osseous tissue (Isaacson et al., 2016). Furthermore, rodent study outcomes are limited; although early signs of woven bone formation which may form HO are observed, the hybrid cortical/cancellous bone structure observed in human HO samples has yet to be replicated. To the authors' knowledge, only one study attempted to produce HO in a large animal model (Walton and Rothwell, 1983). Walton et al. evaluated HO development in ovines and suggested that ectopic bone occurred in only 17% of cases, which failed to achieve the 63%–65% rate of HO formation observed in wounded warfighters (Walton and Rothwell, 1983). However, the study used blunt force rather than blast (i.e., shockwave) trauma, contained limited histological analysis, and the percentage of animals that formed ectopic bone did not simulate battlefield scenarios.

The causative factors of HO development, especially in the case of blast injuries, are not well-known, but are reported to include the following:

(1) A blast/explosion, which generates extensive trauma and potential concomitant brain injury (Isaacson et al., 2016).
(2) Fractured bone, which creates significant bone trauma/micro cracking and disperses loose fragments into the musculature (Isaacson et al., 2016).
(3) Tourniquet use, which alters localized pH and creates a hypoxic environment (Isaacson et al., 2014).
(4) The presence of bacterial biofilms (Pavey et al., 2015). Traumatic injuries in soldiers or civilian patients are likely to be contaminated with bacteria in the biofilm phenotype as opposed to planktonic bacteria (Williams and Costerton, 2012).
(5) Negative Pressure Wound Therapy (NPWT), which may be used post-injury for tissue closure (Forsberg and Potter, 2010). Once a wounded warfighter is transported and stabilized to a forward triage unit, within hours or days, depending on the situation, it is likely that they will begin treatment with NPWT, (i.e., wound vacuum assisted closure (VAC)).

We addressed previous study limitations by assessing traumatic HO formation in a large animal ovine model that mimicked battlefield-relevant and post-traumatic care scenarios. We hypothesized that by using an air impact device (AID) and the above simulated battlefield trauma, HO would form and have similar bone morphology to clinical samples retrieved from wounded warriors (Isaacson et al., 2016).

2. Materials and methods

2.1. Supplies, instruments and reagents

Surgical supplies, reagents, Petri dishes, agar, and brain heart infusion (BHI) broth were purchased from Fisher Scientific (Waltham, MA). Fluids, analgesics, and anesthetics were provided by the University of Utah Comparative Medicine Center. Surgical tools and histological processing equipment/materials were provided by the Bone and Biofilm Research Lab (Salt Lake City, UT). V.A.C. Freedom® Therapy Units were purchased from KCI (San Antonio, TX). Martin® Tornado Air Cannon (Model BB4-12-28, Martin Engineering, Neponset, IL) was donated by Martin Engineering. Calcein green was purchased from Sigma Aldrich (St. Louis, MO). Silica (Si) beads were purchased from Fisher Scientific (Waltham, MA). Scanning electron microscopy (SEM) was performed on a JEOL JSM-6610 (Peabody, MA). Sanderson's Rapid Bone Stain (SRBS) was purchased from Dorn & Hart Microedge Inc. (Loxley, AL).

2.2. Air impact device

A Martin® Tornado Air Cannon with a four-inch valve was used to simulate an improvised explosive device (IED) / rocket propelled grenade (RPG) blast. Parameters of the air blast system were optimized and assessed for this model previously (Williams et al., 2018). In short, the AID delivered a rapid depressurization of air within 0.1 s and incident pressures were estimated to be approximately 588 kPa for a 100 PSI blast; consistent with what may be experienced in the range of a battlefield blast setting based on parameters from the Kingery-Bulmash blast parameter calculator. The AID was assembled based on manufacturer's recommendation and validated for force output previously (Williams et al., 2018).

2.3. Biofilm growth

Biofilms were grown on Si beads (~3 mm in diameter) and used as initial inocula. This modelled the preferred dwelling state of bacteria (in a biofilm) in natural ecosystems, such as on sand particles that contaminate blast-related injuries. Si beads were roughened using 60 grit sandpaper to increase the surface area and improve bacterial adherence/biofilm formation. Bacterial colonies of *Staphylococcus aureus* ATCC 6538 were adjusted to a 0.5 McFarland standard (~7.5×10^7 colony forming units (CFU)/mL) in PBS using a colorimeter. An aliquot of 0.1 mL of the bacterial solution was aseptically inoculated into 9.9 mL of BHI in a 60 mm Petri dish. Ten Si beads were autoclaved, submerged in the inoculated broth, placed in an incubator (37 °C) with an orbital shaker, and rotated at 40 rpm. This rotation rate was experimentally determined to allow fluid motion with minimal Si bead movement so as not to knock off biofilms that formed. Ten milliliters of fresh BHI was replenished every 24 h until a total of ~72 h growth was achieved. Five beads were randomly selected from each batch to inoculate in a sheep. The remaining five beads were used to quantify CFU/bead or to process for secondary electron imaging (SEI) to qualitatively evaluate biofilm morphology on the Si surface (Fig. 1).

2.4. Animal model

All animal work was performed with approval and oversight of the Institutional Animal Care and Use Committee (IACUC) at the University of Utah, and the Animal Care and Use Review Office (ACURO), a
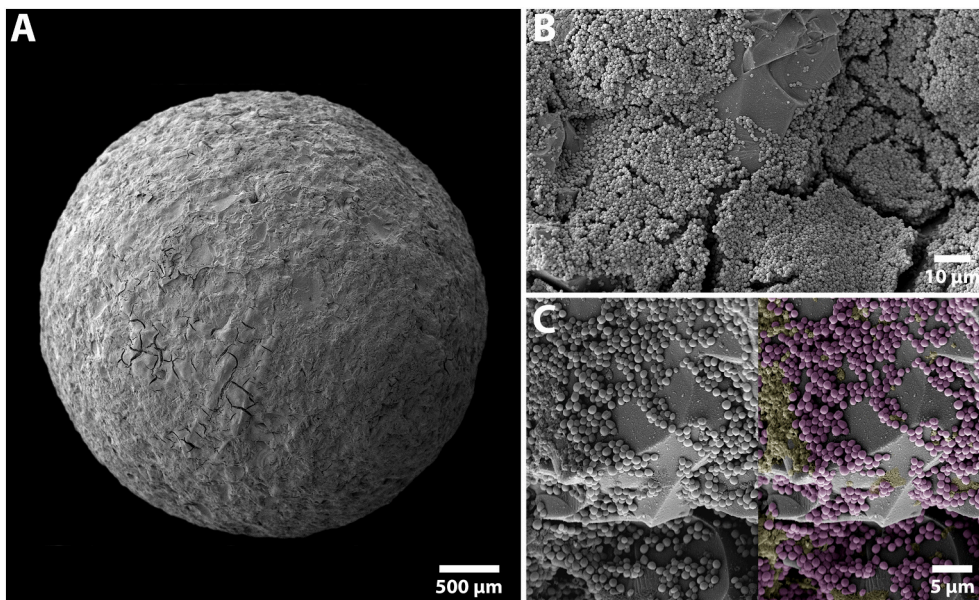
Fig. 1. SEM images demonstrating *S. aureus* ATCC 6538 biofilm formation on a roughened Si bead following 72 h of growth. (A) Overhead view of a roughened Si bead used for inoculation. (B) High power view showing biofilm following 72h of growth. Note the multi-layered biofilm was predominantly located within the concaved regions of the Si beads. (C) Higher magnification showing a multicell layer. The raw SEM image was digitally colored to help define the cells (purple) and extracellular matrix (yellow) against the roughened Si bead surface (grey).

component of the United States Army Medical Research and Development Command Office of Research Protections (USAMRDCORP). Skeletally mature, female Rambouillet sheep (age 1–3 years) were purchased from K Bar Livestock (San Antonio, TX). An *n* = 2 pilot sheep initiated the study to confirm that the AID blast would not result in a bone fracture, and that periosteal disruption, bone feathering, a distal femur bone defect, and tourniquet would be tolerated. In this particular model, we desired for sheep to maintain function and mobility following trauma. Piloting allowed the veterinary staff and researchers to assess safety of the approach and optimize surgical considerations prior to initiating work on main study animals (Table 1).

2.5. Pilot Sheep

A fentanyl patch was placed on a clipped region of the forelimb and secured in place with Elastikon the evening prior to the AID blast and surgical procedure. Sheep were initially sedated with an intravenous (IV) injection of Propofol (3–7 mg/kg) and transferred to a prep room for endotracheal tube intubation. Each was maintained under anesthesia with isoflurane inhalant (0.5%–5.0%). The right hind limb was clipped free of wool/hair up to the rump before transporting to the operating room where the surgical site (lateral thigh) was prepped with betadine/ethanol, draped sterilely, and scrubbed a final time with Chloraprep™ (2% *w/v* chlorhexidine gluconate in 70% *v/v* isopropyl alcohol).

An incision was made in the midshaft region of the right femur. Deep tissue was dissected longitudinally to expose the bone. Surgeons roughened/feathered the periosteum and cortical bone surface using a periosteal elevator and osteotome to simulate bone trauma that might accompany a blast-related injury. A 10 mm bone core was obtained from

the lateral distal femoral condyle through the same incision in the midshaft of the femur. The cored sample contained medullary canal components as well as cortical and trabecular bone chips. The bone core/canal material was broken into small pieces using a rongeur, then mixed with saline to create a slurry. Approximately 2.5 cm^3 of bone slurry were spread onto the disrupted area of the femur to mimic bone chips and host medullary canal components that would be present in a blast-related injury (Fig. 2A).

The incision was sutured closed and covered with a transparent film (Tegaderm®) to limit air entering the incision during the AID blast. The sheep was shielded with a heavy cloth drape (equivalent to a painter's drape) as an additional precaution to limit contamination of the incision site and/or equipment in the room. Foam plugs were placed in each sheep's ears to protect hearing. The nozzle of the AID was situated two inches above the incision site, pressurized to 100 PSI, and discharged. The discharge procedure was repeated a total of three times (Fig. 2B). Fluoroscopic images confirmed the AID blast did not cause bone fracture.

A tourniquet was placed for 45 min to simulate battlefield injury protocol (Fig. 2C). Sheep were recovered and monitored until they were eating, drinking, standing on their own, and resumed weight bearing activity. Pilot sheep were assessed for pain and distress daily by the authors' team and a facility veterinarian. Animals that showed signs of pain or distress were treated with Buprenex (0.005 mg/kg – 0.01 mg/kg) and/or additional fentanyl patches. Pilot sheep were monitored for 12 weeks after which they were euthanized and samples collected for analysis.

2.6. Primary test sheep

Successful completion of pilot sheep warranted advancement to the main study with *n* = 9 animals. The same procedures as described above were performed with four additional factors: (1) the number of AID blasts each sheep received was increased from three to five, (2) three 5 mm defects (drill holes) were created in the midshaft of the femur to allow bone marrow/growth factors to diffuse into the adjacent muscle, (3) biofilm inoculation was used, and (4) wound VAC treatment was initiated (Table 1).

Whereas animals in the pilot test were recovered immediately following tourniquet placement, the *n* = 9 sheep in the main test group remained under anesthesia for biofilm inoculation. To inoculate, the incision line was reopened and five Si beads containing mature biofilms

Table 1
Number of sheep and the surgical procedure(s)/treatment(s) performed on each.

Sheep list			
Groups	Animal #	Time point	Surgical trauma
Pilot	n = 2	12 Weeks	AID (x3), periosteal disruption, bone fragments, and tourniquet
Main	n = 9	24 Weeks	AID (x5), periosteal disruption, transcortical defect, bone fragments, tourniquet, biofilm, and NPWT

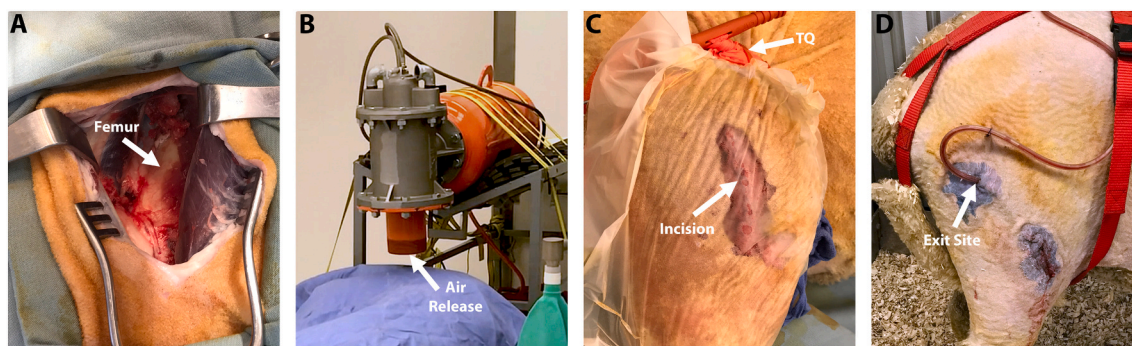NOTE: *n* = 1 sheep from the Main group was euthanized early at 2 weeks.

Fig. 2. Representative photographs demonstrating the surgical approach, and AID blast procedure. (A) Midshaft femoral surgical site with the exposed femur after feathering/roughening. (B) The air release portion of the AID was placed approximately 2″ from the sheep limb. The sheep was covered with a drape to prevent contamination that may have been forced though the incision site, and to protect the equipment in the room. (C) A transparent film allowed for the incision site to remain closed during the AID blast. Following the AID blast, a tourniquet (TQ) was applied close to the hip for ~45 min. (D) An exit site above the main incision allowed the NPWT tubing to be placed subdermally, and still be attached to the external drainage canister.

(biofilm growth described above) were placed directly against the bone midshaft femur adjacent to the created bone chips. Wound VAC foam (V. A.C.® GranuFoam™) was then placed subdermally adjacent to the exposed lateral femur. A subdermal placement was deemed necessary following cadaveric testing, which demonstrated that the lanolin on sheep would not allow for sufficient negative pressure if applied directly to the skin. The foam was wrapped in silicone dressing (ADAPTIC TOUCH™) to reduce tissue integration. A separate secondary incision (~1 cm) was created superior to the original incision line to provide a VAC tubing exit point and connect to the external wound VAC (Fig. 2D). This secondary incision reduced risk of irritation to the surgical site. The secondary incision was sutured closed and sealed with surgical glue (DERMABOND™), creating an air-tight seal for consistent pressure during NPWT.

NPWT was administered at a negative setting of 175 mmHg consistently for 3–7 days; the foam was removed within ~24 h of fluid no longer collecting in the external canister. The wound VAC foam and tubing were surgically removed under anesthesia in a second surgery. Sheep were anesthetized and recovered as described above.

Calcein green (10 mg/kg) was injected in each sheep on two separate occasions. The first injection was given IV 16 days prior to euthanasia; the second was administered 5 days prior to euthanasia. Double injections of calcein green allowed for assessment of bone viability and to determine the rate at which host bone remodeled in regions that were affected by AID trauma, and those that were not (as a baseline). One out of nine sheep did not receive calcein injections as it failed to reach the predetermined endpoint. Clinically HO is shown to usually occur within 3 to 12 weeks after inciting injury, but can also take up to 6 months to present (Sun and Hanyu-Deutmeyer, 2021). Therefore, sheep were humanely euthanized at either 12 or 24 weeks post-surgery with an injection of Beuthanasia D (1 mL/4.5 kg) (Table 1).

2.7. Microbiology, radiography and Micro-CT

Culture swabs were collected at necropsy near the incision line, and proximate to the flank; flank swabs were used to identify bacteria that were naturally present on the sheep. The skin was then prepped to aseptically obtain subdermal samples. A sterile scalpel was used to remove a portion of the skin directly above the midshaft of the femur. Tissue and bone core samples were collected using a biopsy needle (Jamshidi™) in the area where biofilms (on Si beads) were inoculated. Tissue samples directly adjacent to the inoculation site were not collected as the primary outcome measure was to analyze HO formation; we did not want to disrupt potential HO that developed. Tissue samples were weighed, added to 1 mL of PBS, ground in a tissue grinder, vortexed/sonicated and plated using a 10-fold dilution series to quantify

CFU/g tissue.

Limbs were then harvested and radiographed for 9 min in a cabinet X-ray system set at 70 kV. The tibia and patella were disarticulated and the femur was slightly dissected removing only the superficial tissue to allow for the whole femur to fit in a micro-CT chamber. Micro-CT scans were captured with a tube voltage of 90 kVp, tube current 180 µA, and a field-of-view (FOV) of 75 mm, which resulted in 148 µm slices. The scans were 3D-rendered using FIJI (Image J) software to determine presence of ectopic bone. The micro-CT scans were imported into Seg3D (https://sci.utah.edu) to determine bone volume outside the cortical boundary of the periosteum (Isaacson et al., 2011b).

2.8. Histological processing

Femurs were further dissected to remove surrounding soft tissue and bone cut into sections approximately 3 cm thick. Specimens were fixed in 10% neutral buffered formalin, dehydrated in ethanol, infiltrated, and embedded in poly-methyl-methacrylate (PMMA) using our standard PMMA technique (Sanderson and Kitabayashi, 1994; Williams et al., 2019). Polymerized samples were sectioned transversely using a water-cooled saw equipped with a diamond-coated blade resulting in sections with a thickness of about 2–3 mm. Sections were ground and polished to optical finish using a variable-speed grinding wheel, coated with a conductive layer of carbon for ~30 s to allow for imaging by SEM. Imaging used a BSE detector and accompanying JEOL software (Bachus and Bloebaum, 1992). Images were post-processed using Microsoft Research Image Composite Editor (MRICE) to mosaic/stitch BSE images together creating an overhead view (Epperson et al., 2020a; Epperson et al., 2020b).

2.9. Mineral apposition rate and light microscopy

Specimens were further ground, polished and adhered to a plastic slide using EXAKT Technovit 7210 and an EXAKT 402 Precision Adhesive Press. Slides were ground to a thickness of ~50 µm and viewed under a mercury lamp microscope at a magnification of 200× to display the fluorochrome double-labeled bone. The average thickness of the newly mineralized bone was calculated and expressed in units of µm/day (Isaacson et al., 2016; Willie et al., 2004). Mineral apposition rate (MAR) was calculated using the following equation:

$$\text{MAR } [\mu m/day] = \left[\sum x \, \epsilon (\pi/4) \right] \Big/ nt$$

where $\sum x$ = sum of measurements between double labels, ϵ = micrometer calibration factor (microns), $\pi/4$ = obliquity correction factor, n = number of measurements, t = time (days).

Light microscopy was performed after MAR analysis by staining with SRBS (Sanderson and Bachus, 1997). Stained sections were visually examined for evidence of newly-formed osteoid and osteoblast presence.

2.10. Statistical analysis

Outcome measures of the MAR analysis was compared statistically using independent *t*-tests with an alpha level of 0.05.

3. Results

3.1. Biofilm growth, NPWT, and animal monitoring

Biofilm formation on the roughened Si beads was reproducible and created mature biofilms for use as initial inocula. Microbiological quantification showed that on average, one Si bead contained ~7×10^6 CFU for a total of ~3.5×10^7 CFU on five Si beads, which was the amount inoculated in each animal. Biofilm growth on Si beads was confirmed with SEI analysis, and demonstrated uniform coverage across the Si bead surface (Fig. 1).

The "wrapped" wound VAC foam was unproblematic and allowed for continuous negative pressure to be applied subdermally. The surgical glue provided an airtight seal with no signs of irritation. Select sheep demonstrated line blockage that required a line flush, new canisters, and/or new tubing during the NPWT treatment period.

Two contingency sheep were needed throughout the course of the study as two of the sheep suffered a bone fracture ($n = 1$ pilot group & n = 1 main group) in the surgically-treated limbs; fractures were due to a flooring issue and not the AID blast. Despite a rough-textured floor, the straw bedding became slippery. With sudden movements, which are common in sheep, leg fracture occurred. Rubber mats were purchased to increase grip and reduce slipping to mitigate fractures.

Eight out of nine sheep from the main group tolerated the AID blast and surgical trauma with minimal signs of distress. The majority of sheep were lame and limped for approximately one-week post-procedure, in particular during the time the wound VAC was in place. Sheep regained mobility following wound VAC removal and maintained appetite until their predetermined end point. Pain management was administered as needed throughout the course of the study when signs of distress were suspected. One sheep became lethargic with a loss of appetite and was non-weight bearing about two weeks post-AID blast and surgical trauma, and therefore was euthanized early.

3.2. Microbiology, radiography, and micro-CT

Microbiological data showed little to no bacterial growth in the muscle and/or bone regions that were sampled, and overt signs of infection were not present. Gross radiographs of the femoral samples were insufficient to elucidate ectopic bone due to the projection effect. However, radiographs revealed the Si beads containing biofilm migrated toward the hip in select sheep.

The 3D-rendered micro-CT scans from the pilot group revealed jagged ectopic bone stemming from the posterior side in one out of two sheep. Data also indicated that the pilot animal with ectopic bone had a greater degree of feathering/roughening of the bone compared to the pilot sheep that had no signs of ectopic bone. In contrast, all eight sheep from the main group that reached their predetermined endpoint demonstrated ectopic bone growth (8.75 ± 3.52 mm^3) outside the cortical boundary of the periosteum on the shaft of the femur (Fig. 3 & Table 2). In three out of eight sheep, reactive bone growth was observed on the distal condyles stemming from the medial and lateral sides. This growth appeared to be unrelated to the bone cores that were collected to produce the bone chip slurry. No growth/bone response was observed on the contra-lateral limb suggesting the trauma and AID blast was localized only to the surgically operated limb.

Table 2
Volume of bone outside of the cortical boundary of the periosteum.

Volume of ectopic bone	
Specimen #	Volume (mm^3)
Pilot - a	–
Pilot - b	5.0658
1	14.9837
2	6.0912
3	9.7224
4	6.4713
5	6.4951
6	N/A
7	13.1463
8	6.8444
9	6.2231
Mean	8.75
Stdev	3.52
Median	6.67
Min	6.09
Max	14.98

Note: Mean volume excludes pilot data.

Sagittal Plane — **A** — Ectopic Bone / No Response

Transverse Plane — **B** — Periosteal Response / Bone Loss / Ectopic Bone / Si Beads
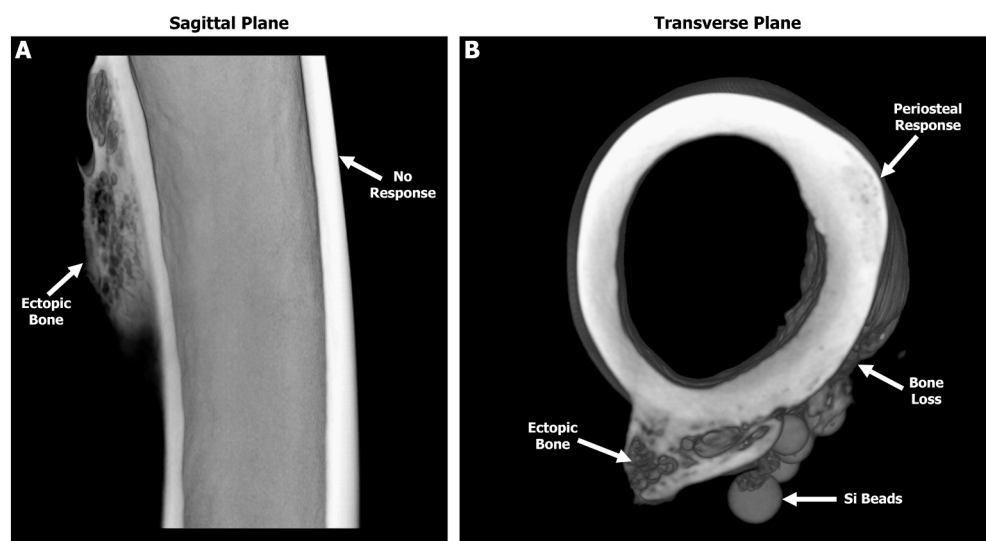
Fig. 3. Representative three-dimensional reconstructed micro-CT scans from a sheep of the main study group revealing ectopic bone growth on the posterior side of the femur. (A) Sagittal plane showing the posterior ectopic bone with a trabecular-like structure. The anterior cortical wall demonstrated no obvious signs of a bone response. (B) Transverse plane similarly revealing that the ectopic bone has a trabecular-like structure with a cortical shell. Note the smooth periosteal response on the lateral side as well as the bone loss adjacent to the Si beads.

3.3. SEM BSE analysis

BSE images provided a more detailed analysis of bone response compare to radiographic or micro-CT data. All specimens from sheep in the main study group demonstrated a significant bone response, yet the level of response and morphology varied from sheep to sheep. Overall, bone was still in its native plexiform structure in the anterior and medial regions, suggesting that the AID blast did not elicit a response in those regions. This was in stark contrast to the lateral region where the bone was roughened/feathered, which demonstrated osteonal remodeling in the mid-cortex region along with a smooth periosteal response extending approximately 1–2 mm from the outer boundary of the cortical bone (Fig. 4). This periosteal response was observed in all sheep.

The transcortical 5 mm drill holes had osseous unions that bridged the defects with minimal external growth within the canal or outside the cortical boundary (Fig. 4). When the Si biofilm beads were in close approximation to the bone, significant bone resorption was observed directly beneath them. This resorption resulted in endosteal wall thickening, as well as promoted external bone growth in the adjacent regions (Fig. 4).

BSE data showed that five out of eight sheep from the main study group exhibited ectopic bone that resembled human HO; bone growth was a complex hybrid of trabecular-like structure with osteon remodeling, as well as hyper-mineralized regions (Figs. 5 & 6). The observed

bone growth differed from the smooth periosteal and endosteal responses present predominantly on the lateral side (Figs. 4 & 5). Fluorochrome double labels confirmed these differential findings (see below).

The single sheep that was euthanized early (approximately two weeks post-operative) had signs of woven bone stemming from loose bone chips within the medullary canal. Overall, no significant bone response due to the AID blast was observed as the native plexiform bone structure was still present in all regions nearly two weeks post-AID blast. This suggests that the trauma-induced bone modeling/remodeling was still in a quiescent state and that a significant bone response may not begin until after two weeks post-trauma.

3.4. MAR and light microscopy analysis

Fluorochrome label analysis demonstrated six distinct areas of bone remodeling. Standard osteon remodeling was also observed in the unaffected mid-cortex region of the cortical bone, within the new bone growth of the periosteal response, in the osseous unions of the 5 mm defects and at the linea aspera interface. In contrast, the area affected by the Si biofilm beads demonstrated a sheet-like layering structure of fluorochrome labels signaling a biofilm infection bone response as describe by Williams et al. (Williams et al., 2012). Ectopic bone that resembled human HO demonstrated distinct double labels similar to
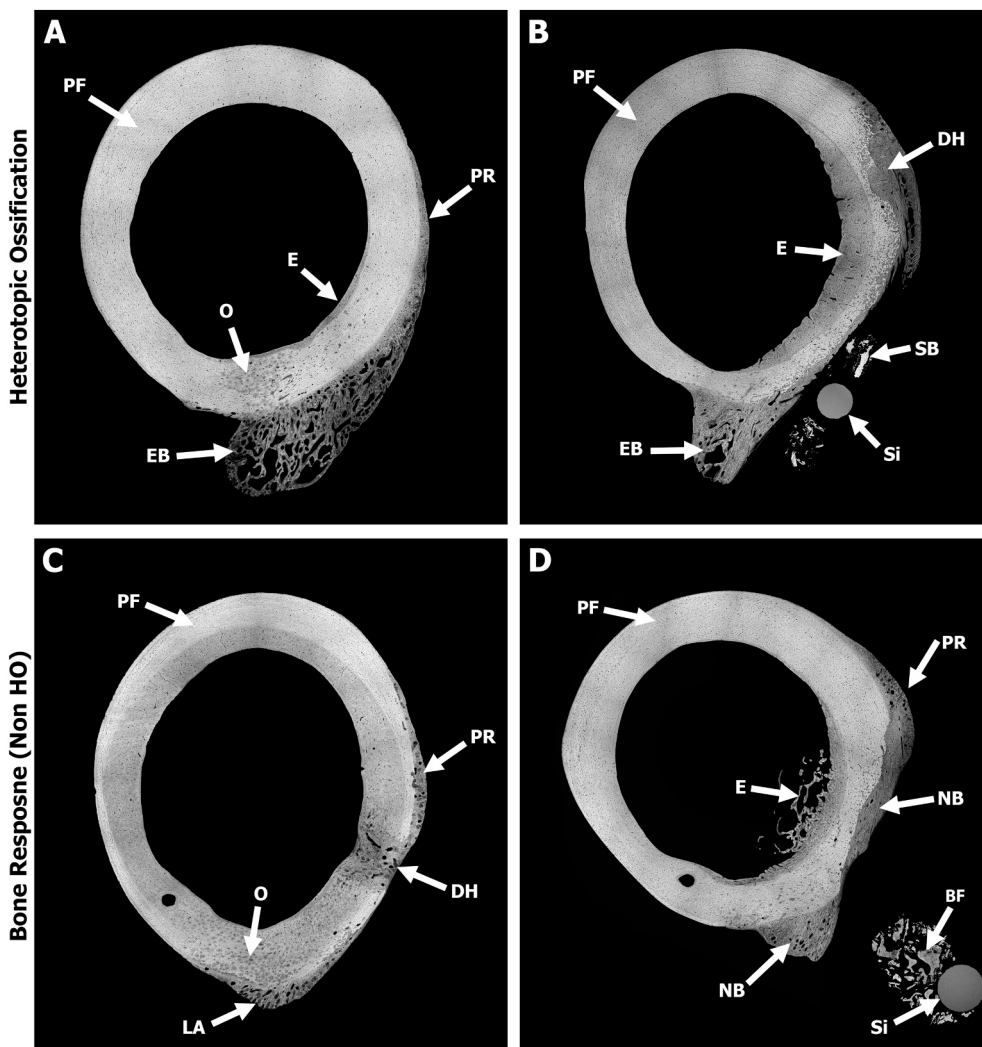

Fig. 4. Representative SEM BSE images stitched together using MRICE to create an overhead cross-sectional view demonstrating HO and non-HO bone responses. Gray = bone and Black = soft tissue/pore space. (A) Sheep #7 showed HO-structured ectopic bone (EB) stemming from the posterior side along with osteonal remodeling (O) near the midcortex. Note the smooth periosteal response (PR) observed on the lateral side where the bone was roughened prior to the AID blast. A region of endosteal (E) remodeling was also observed within the canal adjacent to the drill hole on the lateral side. The anterior and medial regions showed no signs of significant bone response due to the AID blast as the native plexiform (PF) bone structure was still present. (B) Sheep #1 demonstrated similar results as Sheep #7. Image shows the HO ectopic bone (EB) and new bone growth stemming from the drill hole (DH) defect, which may have been influenced by the inoculated biofilm from the Si bead (Si). Endosteal (E) thickening appeared to be caused by biofilm resorbing the periosteum. Biofilms also appeared to form sequestrum bone (SB) on the lateral side. (C) Sheep #5—one out of the three sheep that did not contain the HO structure bone response. New bone growth is observed outside the normal boundary of the cortical bone on the posterior side at the linea aspera (LA) region along with a smooth periosteal response (PR) on the lateral side due to the bone roughening/periosteal disruption. (D) Sheep #3 demonstrated similar results as Sheep #5, with new bone (NB) growth at the linea aspera interface in addition to new bone growth filling in previously resorbed cortex due to the inoculated biofilm. Note the smooth periosteal response (PR) observed on the lateral side as well as the loose bone fragments (BF) around the Si beads (Si).
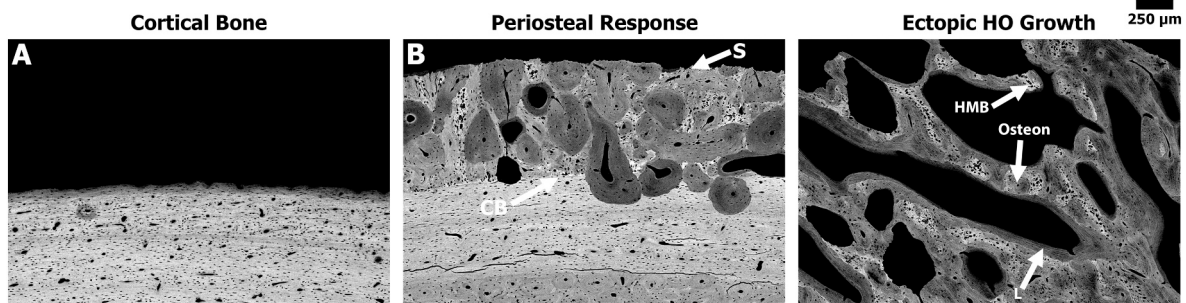
Fig. 5. Representative high magnification BSE images of the different bone responses observed due to the surgical trauma and/or AID blasts. Gray = bone and Black = soft tissue/pore space. (A) Native sheep cortical bone from the anterior regions remained in the plexiform state exhibiting no significant response associated with the AID blast. (B) Periosteal response (darker gray) extended from the cortical boundary (CB) on the lateral side of the femur where the bone feathering/roughening occurred. Note the smooth/dense (S) nature of the periosteal response in this region. (C) Ectopic HO bone growth showed a complex hybrid bone structure that resembles human HO. Note the ectopic bone demonstrated a trabecular-like structure with osteon (O) remodeling, areas of hyper-mineralized bone (HMB), as wells as long non-circular lamellae lines (L) at the bone seams.
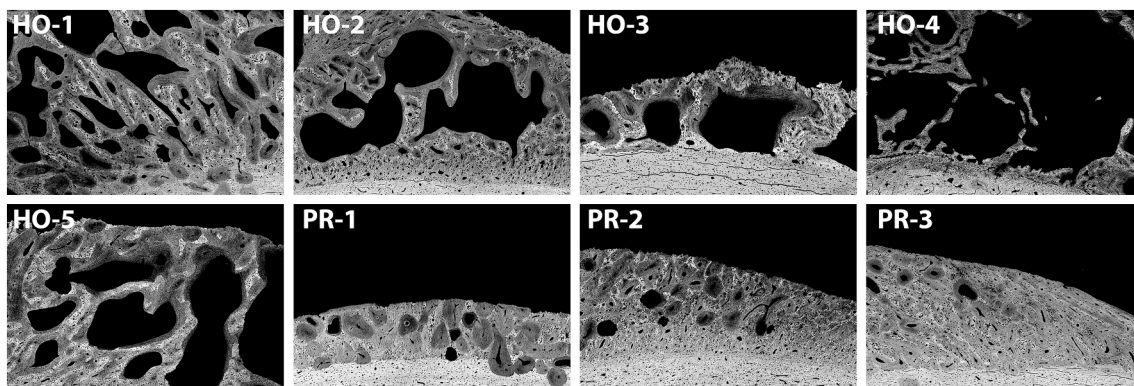

Fig. 6. Representative high magnification BSE images from each sheep demonstrating that 5 out of 8 sheep exhibited the complex, jagged HO bone structure, while the bone growth in the remaining 3 sheep was predominantly a smooth periosteal reaction (PR).

trabecular modeling, which was in stark contrast to the standard circular osteonal remodeling in the regions described above (Fig. 7). Double label analysis revealed that MAR outcomes were not statistically significant (Table 3) when comparing the unaffected host cortical bone (0.9 ± 0.3 μm/day) to the periosteal response (0.9 ± 0.3 μm/day) and biofilm (1.4 ± 0.4 μm/day) regions. However, MARs between bridge regions of the five mm drill holes (1.5 ± 0.3 μm/day), linea aspera (1.5 ± 0.4 μm/day), and the ectopic HO bone (1.6 ± 0.4 μm/day) were all significantly different ($p \leq 0.0343$) compared to the MAR of unaffected host cortical bone. The ectopic bone that resembled human HO had the highest MAR and was $1.7\times$ greater than the MAR of the double labels within the boundary of the unaffected host cortical bone (Table 3).

Light microscopy analysis confirmed the presence of osteoblasts and osteoid at the fluorochrome labeled regions, suggesting that ectopic HO bone was still actively modeling 24 weeks post-AID and surgical trauma (Fig. 8).

4. Discussion

HO remains a major concern with traumatic injuries, in particular blast injuries that result in limb loss to wounded warriors. The removal of HO and recurrence in injured service members are challenging given comorbidities and severity of the injuries sustained. Due to the cause of HO being relatively unknown, preventive measures are limited. Forsberg et al., stated "one of the challenges preventing advances in this field has been the lack of robust animal models for HO" (Dudek et al., 2003). This study addressed this limitation by establishing a large animal model that produced HO in a blast-related scenario. Outcomes replicated what

is observed clinically as five out of eight (63%) sheep showed a hybrid HO bone structure.

Specifically, human HO excised from wounded warfighters demonstrated a hybrid cortical/cancellous morphology with trabecular-like bone structure, osteon remodeling, and varying degrees of mineralization (Isaacson et al., 2011a; Isaacson et al., 2016). In this sheep model, and clinical samples analyzed previously, the hybrid cortical/cancellous morphology of HO bone was elucidated using BSE imaging and SRBS in PMMA-embedded samples. Thus, a primary takeaway is that HO bone may be more accurately identified by BSE analysis with histological sections that are not decalcified.

The $n = 3$ sheep in the main study portion that did not form a hybrid HO-like bone structure did still produce ectopic bone; however, it was more similar to a periosteal reaction and/or a bone response that may have derived from infection-induced osteolysis via the inoculated biofilm. Fluorochrome data indicated that the bone was still modeling/remodeling, which begs the question of whether the time frame was too short; would HO have formed if sheep were monitored for a longer period of time?

Fluorochrome labels further differentiated unique bone responses observed by BSE imaging; the ectopic bone that resembled human HO demonstrated distinct double labels that mimicked trabecular modeling. This was in stark contrast to the standard circular osteonal remodeling that was present mid-cortex, in the periosteal response, osseous unions of the 5 mm defects, and linea aspera interfaces. The area affected by biofilm was unique with a sheet-like layering structure and correlated with a biofilm-induced bone response (Williams et al., 2012).

Notably, this outcome indicated that despite limited bacterial growth
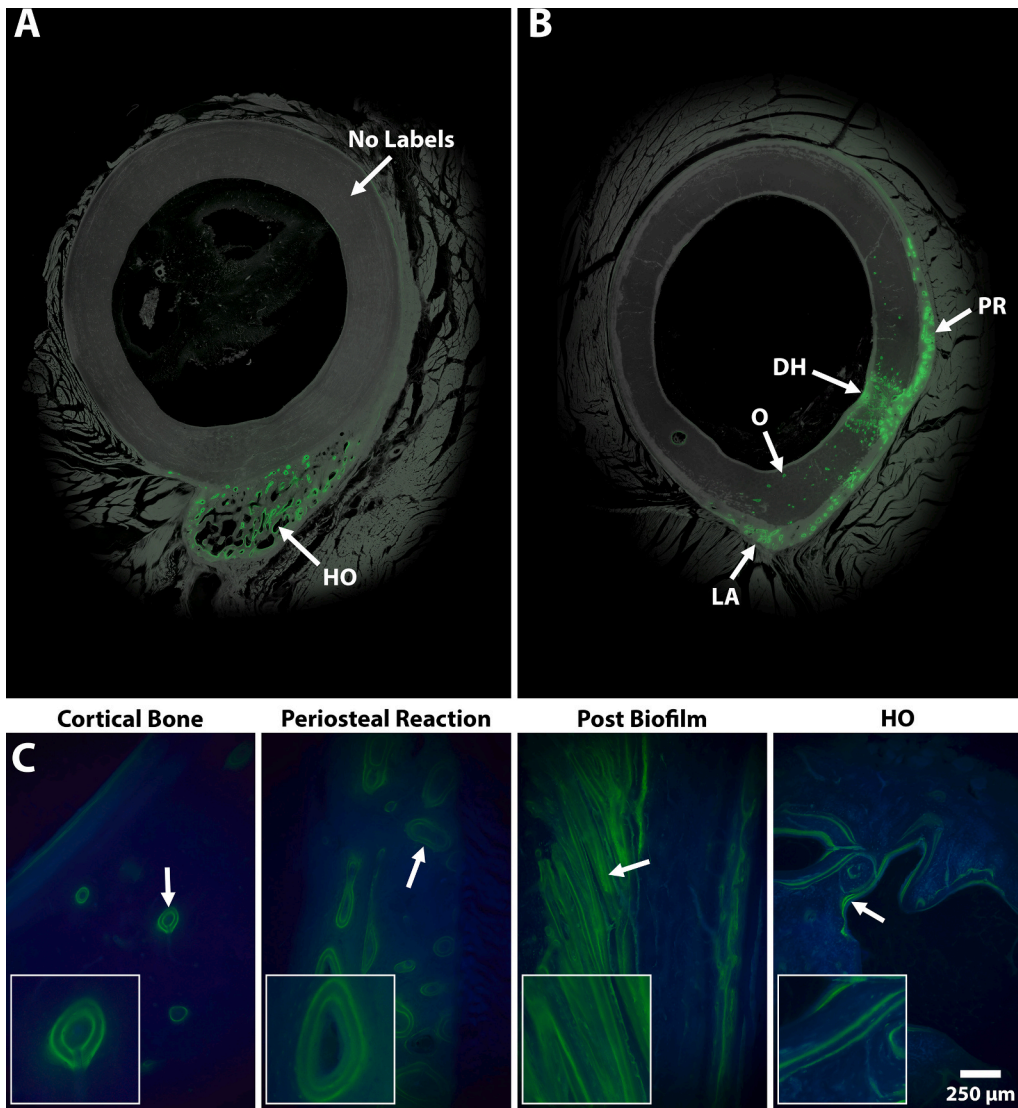
Fig. 7. Representative images showing the different bone remodeling structures as a result of fluorochrome double labels (green). (A) Overhead view demonstrating that HO modeling was independent with minimal effect to the host bone, which had no labels. (B) Overhead view demonstrating bone modeling at the linea aspera (LA), periosteal reaction (PR), and drill hole (DH) defect regions. Osteonal (O) remolding was also observed mid-cortex. (C) Images showing a high magnification (100×) view of the different bone remodeling structures. Host cortical bone had standard osteonal remodeling comprised of small circular double labels. The periosteal modeling contained large circular double labels, similar to the host cortical bone. Remodeling near biofilm inocula demonstrated sheet-like double labels filling in the previously resorbed bone. Ectopic bone modeling resembled human HO similar to trabecular remodeling with linear double labels predominantly at the bone seams.

Table 3
Outcomes of the MAR (µm/day) data.

Mineral apposition rate (µm/day)						
Region	Mean	Stdev	Median	Minimum	Maximum	P Value
Cortical bone	0.9	0.3	0.8	0.6	1.3	
Periosteal	1.2	0.6	1.5	0.6	1.7	
Defect (drill hole)	1.5	0.2	1.5	1.2	1.6	
Biofilm	1.4	0.4	1.5	0.9	1.7	
Linea aspera	1.5	0.4	1.4	1.0	2.0	
HO	1.6	0.4	1.6	1.0	2.1	
Cortical vs defect						**0.0186**
Cortical vs linea aspera						**0.0343**
Cortical vs HO						**0.0088**

Note. Only comparisons considered to be statistically significant (bold) are shown ($P < 0.05$).

Fig. 8. Representative light microscopy micrograph stained with SRBS showing a region of ectopic bone (pink) growth extending into the adjacent muscle and tissue (blue). New bone (NB) growth was observed in the adjacent vascularized granular tissue (VGT), as well as osteoblast (OB) activity at the bone seams.

in cultured samples, an infection response was present in various ectopic bone regions. Thus, limited microbiological culture data was likely a result of sampling location as opposed to lack of bacterial presence. This was not a concern as the primary outcome measure was a determination of HO, not infection. However, consistent with previous studies in which
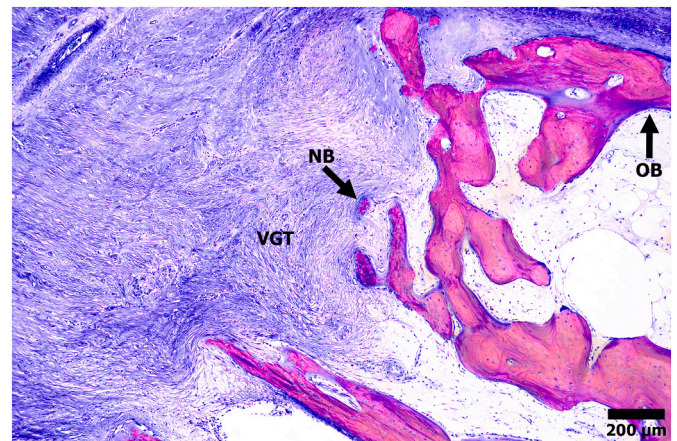
we have used biofilms as initial inocula, only one sheep received a course of antibiotics mid-study to manage swelling and lameness, thus indicating that biofilms as initial inocula produced a low-lying, quiescent infection that had minimal effect on animal well-being.

MAR data demonstrated a bone remodeling rate $1.7 \times$ higher than the host cortical bone 24 weeks post-trauma. This coincides with human HO remodeling rates and suggests that HO was still actively modeling and advancing into the muscle (Isaacson et al., 2016).

Limitations of the study include the lack of bone fracture, amputation (which has demonstrated increased HO formation in rodents) (Polfer et al., 2015), thermal injuries (burns) (Foster et al., 2017) and that the localized AID blast did not influence brain injury. These limitations might explain the low volume of HO exhibited compared to HO excised in wounded warriors. Additionally, individual factors (i.e. AID blast only, bacteria only) were not tested. Different time points may also have been beneficial to observe the early bone response. This early bone response would be required to determine if the HO growth followed a similar formation pattern as to what is observed clinically. Additionally, it would be important to determine when the HO growth would become quiescent. Additional studies are currently ongoing (including a sheep model of HO formation following blast-related trauma and amputation) to address these limitations to continue to advance the model, thus increasing the volume of HO bone to be more clinically relevant to the amount of HO observed in wounded warriors.

5. Conclusion

Our hypothesis that an AID blast and simulated battlefield trauma would result in HO growth was supported in 63% of ovines. Although all sheep demonstrated ectopic bone growth, only 5 out of 8 revealed the complex HO structure observed in human HO excised from wounded warriors. This data suggested that BSE and undecalcified histological analyses on samples embedded in PMMA may assist in determining the hybrid bone morphology of HO due to the ability of BSE to more readily identify the varied mineralization and structural difference observed in traumatic-induced HO.

CRediT authorship contribution statement

RTE performed histological analysis and drafted the manuscript. BK & JMM supported histological analysis and manuscript preparation. PFP & JS supported study design and manuscript preparation. DLR & REO performed the surgical procedure and supported manuscript preparation. DLW and BMI developed the study design, managed overall aspects, secured funding, supported histological analysis, and manuscript preparation.

Declaration of competing interest

No benefits in any form have been or will be received from a commercial party related directly or indirectly to the subject of this article. There is no COI to report.

Acknowledgments

References

Atkinson, G.J., Lee, M.Y., Mehta, M.K., 2010. Heterotopic ossification in the residual lower limb in an adult nontraumatic amputee patient. Am. J. Phys. Med. Rehabil. 89, 245–248. https://doi.org/10.1097/PHM.0b013e3181c5657c.

Bachus, K., Bloebaum, R., 1992. Projection effect errors in biomaterials and bone research. Cells Mater. 2, 8.

Balboni, T.A., Gobezie, R., Mamon, H.J., 2006. Heterotopic ossification: pathophysiology, clinical features, and the role of radiotherapy for prophylaxis. Int. J. Radiat. Oncol. Biol. Phys. 65, 1289–1299. https://doi.org/10.1016/j.ijrobp.2006.03.053.

Bayley, S.J., 1979. Funnybones: a review of the problem of heterotopic bone formation. Orthop. Rev. 8, 113–120.

Brown, K.V., et al., 2010. Comparison of development of heterotopic ossification in injured US and UK armed services personnel with combat-related amputations: preliminary findings and hypotheses regarding causality. J. Trauma 69 (Suppl. 1), S116–S122. https://doi.org/10.1097/TA.0b013e3181e44cc7.

Dudek, N.L., DeHaan, M.N., Marks, M.B., 2003. Bone overgrowth in the adult traumatic amputee. Am. J. Phys. Med. Rehabil. 82, 897–900. https://doi.org/10.1097/01.PHM.0000087459.94599.2D.

Epperson, R.T., Barg, A., Williams, D.L., Saltzman, C.L., 2020. Histological analysis of a retrieved porous tantalum total ankle replacement: a case report. JBJS Case Connect 10, e0379. https://doi.org/10.2106/jbjs.Cc.19.00379.

Epperson, R.T., Mangiapani, D., Bloebaum, R.D., Hofmann, A.A., 2020. Bone ingrowth comparison of irregular titanium and cobalt-chromium coatings in a translational cancellous bone model. J Biomed Mater Res B Appl Biomater 108, 1626–1635. https://doi.org/10.1002/jbm.b.34509.

Errico, T.J., Fetto, J.F., Waugh, T.R., 1984. Heterotopic ossification. incidence and relation to trochanteric osteotomy in 100 total hip arthroplasties. Clin. Orthop. Relat. Res. 138–141.

Forsberg, J.A., Potter, B.K., 2010. Heterotopic ossification in wartime wounds. J. Surg. Orthop. Adv. 19, 54–61.

Forsberg, J.A., et al., 2009. Heterotopic ossification in high-energy wartime extremity injuries: prevalence and risk factors. J. Bone Joint Surg. Am. 91, 1084–1091. https://doi.org/10.2106/JBJS.H.00792, 91/5/1084 [pii].

Foster, N., Kornhaber, R., McGarry, S., Wood, F.M., Edgar, D.W., 2017. Heterotopic ossification in adults following a burn: a phenomenological analysis. Burns 43, 1250–1262. https://doi.org/10.1016/j.burns.2017.03.001.

Henrot, P., et al., 2000. Imaging of the painful lower limb stump. Radiographics 20 (Spec No), S219–S235. https://doi.org/10.1148/radiographics.20.suppl_1.g00oc14s219.

Isaacson, B.M., Stinstra, J.G., MacLeod, R.S., Pasquina, P.F., Bloebaum, R.D., 2010. Developing a quantitative measurement system for assessing heterotopic ossification and monitoring the bioelectric metrics from electrically induced osseointegration in the residual limb of service members. Ann. Biomed. Eng. 38, 2968–2978. https://doi.org/10.1007/s10439-010-0050-2.

Isaacson, B.M., Brown, A.A., Brunker, L.B., Higgins, T.F., Bloebaum, R.D., 2011. Clarifying the structure and bone mineral content of heterotopic ossification. J. Surg. Res. 167, e163–e170. https://doi.org/10.1016/j.jss.2010.12.047.

Isaacson, B.M., et al., 2011. An evaluation of electrical stimulation for improving periprosthetic attachment. J Biomed Mater Res B Appl Biomater 97, 190–200. https://doi.org/10.1002/jbm.b.31803.

Isaacson, B.M., Swanson, T.M., Potter, B.K., Pasquina, P.F., 2014. Tourniquet use in combat-injured service members: a link with heterotopic ossification? Orthop. Res. Rev. 6, 27.

Isaacson, B.M., et al., 2016. Link between clinical predictors of heterotopic ossification and histological analysis in combat-injured service members. J. Bone Joint Surg. Am. 98, 647–657. https://doi.org/10.2106/JBJS.15.00895.

Marcus, R., Feldman, D., Dempster, D., Luckey, M., Cauley, J., 2013. Academic Press, 362.

Ohlmeier, M., et al., 2019. Heterotopic ossification in orthopaedic and trauma surgery: a histopathological ossification score. Sci. Rep. 9, 18401. https://doi.org/10.1038/s41598-019-54986-2.

Pavey, G.J., et al., 2015. Bioburden increases heterotopic ossification formation in an established rat model. Clin. Orthop. Relat. Res. 473, 2840–2847. https://doi.org/10.1007/s11999-015-4272-3.

Polfer, E.M., et al., 2015. The development of a rat model to investigate the formation of blast-related post-traumatic heterotopic ossification. Bone Joint J 97-b, 572–576. https://doi.org/10.1302/0301-620x.97b4.34866.

Potter, B., et al., 2010. In: Pasquina, P., Cooper, R. (Eds.), Rehabilitation of Combat Casualties With Limb Loss. Borden Institute, pp. 153–190.

Potter, B.K., Scoville, C.R., 2006. Amputation is not isolated: an overview of the US Army amputee patient care program and associated amputee injuries. J. Am. Acad. Orthop. Surg. 14, S188–S190.

Potter, B.K., Burns, T.C., Lacap, A.P., Granville, R.R., Gajewski, D.A., 2007. Heterotopic ossification following traumatic and combat-related amputations. prevalence, risk factors, and preliminary results of excision. J. Bone Joint Surg. Am. 89, 476–486. https://doi.org/10.2106/JBJS.F.00412.

Rossier, A.B., et al., 1973. Current facts on para-osteo-arthropathy (POA). Spinal Cord 11, 36–78. https://doi.org/10.1038/sc.1973.5.

Sanderson, C., Bachus, K.N., 1997. Staining technique to differentiate mineralized and demineralized bone in ground sections. J. Histotechnol. 20, 119–122. https://doi.org/10.1179/his.1997.20.2.119.

Sanderson, C., Kitabayashi, L.R., 1994. Parallel experience of two different laboratories with the initiator perkadox 16 for polymerization of methylmethacrylates. J. Histotechnol. 17, 343–348. https://doi.org/10.1179/his.1994.17.4.343.

Shehab, D., Elgazzar, A.H., Collier, B.D., 2002. Heterotopic ossification. J. Nucl. Med. 43, 346–353.

Shore, E.M., Kaplan, F.S., 2010. Inherited human diseases of heterotopic bone formation. Nat. Rev. Rheumatol. 6, 518–527. https://doi.org/10.1038/nrrheum.2010.122.

Sun, E., Hanyu-Deutmeyer, A.A., 2021. StatPearls. StatPearls Publishing Copyright © 2021, StatPearls Publishing LLC.

van Leeuwen, R.J., Kraal, T., Scholtens, S., Visser, G., 2016. A large heterotopic ossification in a 25 years old laparotomy scar. Quant. Imaging Med. Surg. 6, 470–473. https://doi.org/10.21037/qims.2016.07.05.

Walton, M., Rothwell, A.G., 1983. Reactions of thigh tissues of sheep to blunt trauma. Clin. Orthop. Relat. Res. 273–281.

Williams, D.L., Costerton, J.W., 2012. Using biofilms as initial inocula in animal models of biofilm-related infections. J Biomed Mater Res B Appl Biomater 100, 1163–1169. https://doi.org/10.1002/jbm.b.31979.

Williams, D.L., et al., 2012. Experimental model of biofilm implant-related osteomyelitis to test combination biomaterials using biofilms as initial inocula. J. Biomed. Mater. Res. A 100, 1888–1900.

Williams, D.L., et al., 2018. System setup to deliver air impact forces to a sheep limb: preparation for model development of blast-related heterotopic ossification. JMIR Res Protoc 8, e12107. https://doi.org/10.2196/preprints.12107.

Williams, D.L., et al., 2019. In vivo analysis of a first-in-class tri-alkyl norspermidine-biaryl antibiotic in an active release coating to reduce the risk of implant-related infection. Acta Biomater. https://doi.org/10.1016/j.actbio.2019.01.055.

Willie, B., Bloebaum, R., Bireley, W., Bachus, K., Hofmann, A., 2004. Determining relevance of a weight-bearing ovine model for bone ingrowth assessment. J. Biomed. Mater. Res. A 69A, 567–576.